

Comparison of two algorithms in the automatic segmentation of blood vessels in fundus images

Robert LeAnder, Myneni Sushma Chowdary, Swapnasri Mokkapati, and Scott E Umbaugh

ABSTRACT

Effective timing and treatment are critical to saving the sight of patients with diabetes. Lack of screening, as well as a shortage of ophthalmologists, help contribute to approximately 8,000 cases per year of people who lose their sight to diabetic retinopathy, the leading cause of new cases of blindness [1] [2]. Timely treatment for diabetic retinopathy prevents severe vision loss in over 50% of eyes tested [1]. Fundus images can provide information for detecting and monitoring eye-related diseases, like diabetic retinopathy, which if detected early, may help prevent vision loss. Damaged blood vessels can indicate the presence of diabetic retinopathy [9]. So, early detection of damaged vessels in retinal images can provide valuable information about the presence of disease, thereby helping to prevent vision loss.

Purpose: The purpose of this study was to compare the effectiveness of two blood vessel segmentation algorithms. **Methods:** Fifteen fundus images from the STARE database were used to develop two algorithms using the CVIPtools software environment. Another set of fifteen images were derived from the first fifteen and contained ophthalmologists' hand-drawn tracings over the retinal vessels. The ophthalmologists' tracings were used as the "gold standard" for perfect segmentation and compared with the segmented images that were output by the two algorithms. Comparisons between the segmented and the hand-drawn images were made using Pratt's Figure of Merit (FOM), Signal-to-Noise Ratio (SNR) and Root Mean Square (RMS) Error. **Results:** Algorithm 2 has an FOM that is 10% higher than Algorithm 1. Algorithm 2 has a 6%-higher SNR than Algorithm 1. Algorithm 2 has only 1.3% more RMS error than Algorithm 1. **Conclusions:** Algorithm 1 extracted most of the blood vessels with some missing intersections and bifurcations. Algorithm 2 extracted all the major blood vessels, but eradicated some vessels as well. Algorithm 2 outperformed Algorithm 1 in terms of visual clarity, FOM and SNR. The performances of these algorithms show that they have an appreciable amount of potential in helping ophthalmologists detect the severity of eye-related diseases and prevent vision loss.

INTRODUCTION

Diabetes causes Diabetic Retinopathy (DR) by damaging the smaller retinal blood vessels which may lead to blindness. DR has three stages: Background Diabetic Retinopathy (BDR), Proliferate Diabetic Retinopathy (PDR) and Severe Diabetic Retinopathy (SDR) [3]. BDR is characterized by arteries that swell, weaken, become damaged and leak blood and serum deposits into the macula (center of the retina). These deposits of protein called exudates make the macula swell and decrease vision. The PDR stage is characterized by problems with retinal circulation and consequent oxygen deprivation. The retinal circulatory system then tries to compensate for circulation loss by re-vascularizing the retinal surface with an abnormal growth of new, fragile vessels to avoid retinal cellular suffocation. However, this process leaks blood into the jelly-filled volume of the eye, thereby increasing pressure and decreasing vision. [3] The purpose of this study is to compare the effectiveness of two blood-vessel-segmentation algorithms. The objective is to choose the best algorithm for refinement and application in the automatic detection of retinal blood vessels damaged in the BDR stage – the earliest stage of DR.

MATERIALS AND METHODS

A. MATERIALS

Image Database: Fifteen color fundus images were collected from the STructured Analysis of the Retina (STARE) image database.

Hand-Drawn Images: Fifteen ophthalmologists' hand-drawn tracings of the retinal blood vessels in the color fundus images mentioned above were downloaded from the STARE database. These were to be used as the “gold standard” of vessel segmentation and compared to the algorithm-output images to make an assessment of the segmentation effectiveness of those algorithms.

Software: The CVIPtools (Computer Vision and Image Processing) software package was used to perform the image processing operations as well as to calculate the differences between the hand-drawn images and the segmented images output by the two algorithms. Calculation tools in CVIPtools included Pratt's Figure of Merit, Signal-to-Noise Ratio and Root Mean Square Error.

B. METHODS

Fundus image preprocessing and blood vessel segmentation proceeded as follows:

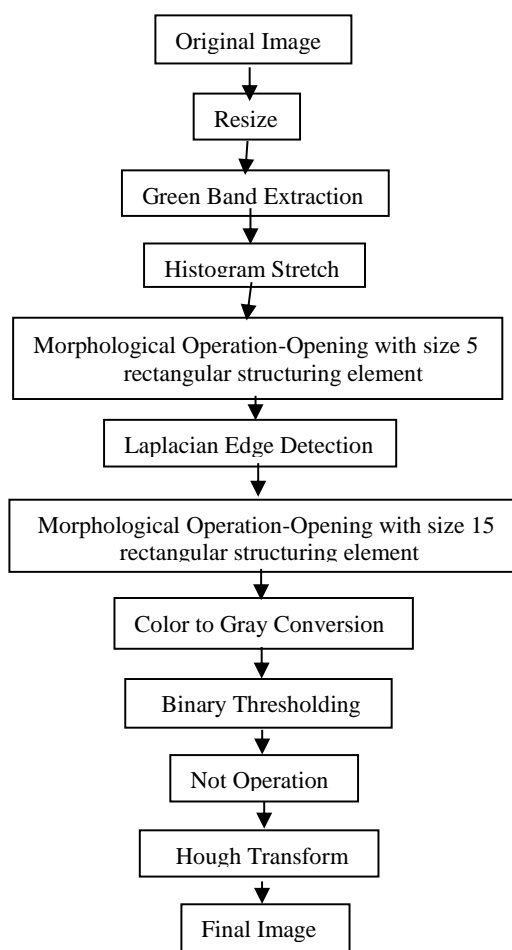


Fig. 1. Flowchart for automatic blood-vessel-segmentation Algorithm 1.

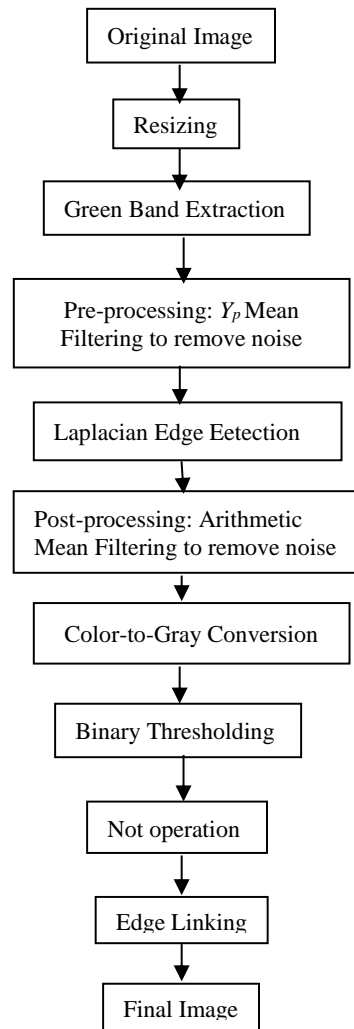


Fig. 2. Flowchart for automatic blood-vessel-segmentation Algorithm 2.

Preprocessing (Algorithms 1 & 2): The images were resized from 150x130 to 300x260 pixels to provide greater visual clarity (See Figures 3, 4, 14 and 15).



Fig 3. Original fundus image A (150x130).

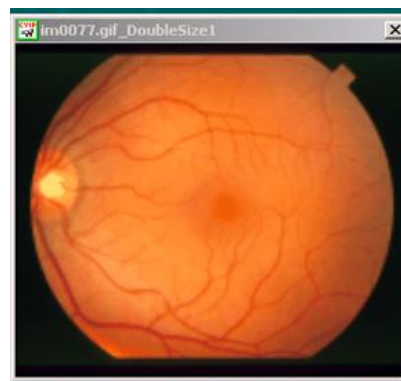


Fig 4. Resized original image A (300x260).

The green band was extracted from the color fundus images because it contains the greatest amount of contrast, is less affected by variations in illumination and consequently has the most pertinent visual information [8] (See Figures 5 and 16).



Fig 5. Preprocessing step 1. Extraction of the green band from the resized, original, color image helped enhance image details.



Fig 6. Preprocessing step 2: A histogram stretch of the green band image helped enhance contrast.



Fig 7. Morphological filtering operation. An opening operation with a size-5 rectangular structuring element smoothed the vessels' geometries.

Both algorithms employ a Laplacian edge detector as the primary segmentation tool. The principal differences between the algorithms occur in preprocessing between green band extraction and edge detection. At that juncture, Algorithm 1 employs a histogram stretch to increase contrast between the blood vessels and the background (fundus) and consequently increased blood vessel details and resolution. (See Figure 6) [4]. Instead of a histogram stretch, Algorithm 2, employed a Y_p mean filter to remove noise and to smooth the images [4] (See Figure 17). The Y_p mean filter was chosen over other filters that were tried because it provided better noise removal and image smoothing. The Y_p mean filter is expressed as:

$$Y_p = \frac{1}{N} \sum_{d(r,c) \in W} d(r,c)$$

where $d(r,c)$ are the degraded image pixel values, N is the filter window size and W is the current $N \times N$ window centered at $d(r,c)$ [4].

Morphological Filtering (Algorithm 1): In Algorithm 1, after histogram stretching, a morphological filter having a small (size-5) structuring element was used to perform an opening operation. (See Fig. 7). An opening operation consists of image object erosion followed by dilation. It eliminates all pixels in regions that are too small to contain the structuring element, thereby “smoothing” the vessels’ shapes and enhancing their fundamental geometric properties [4]. “Opening” opens up (expands) holes and erodes edges. Also, due to the ability of the opening operation to remove small noise points, noise patterns were removed. Opening also helped fill in small holes in the vessels while connecting disjoint parts of the vessels that are supposed to be connected [4].

Edge Detection (Algorithms 1 & 2): Both Algorithms 1 and 2 employed a Laplacian edge detector to extract the blood vessels’ features from the image (See Figs. 8 and 18).

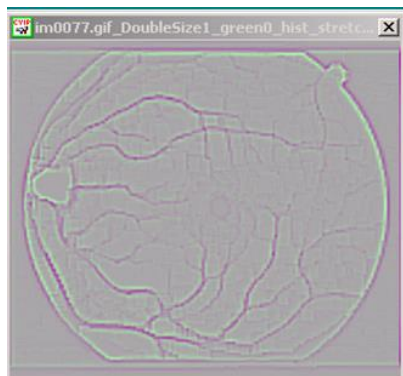


Fig 8. Edge detection.
Edges of the morphologically-filtered image were detected using a Laplacian edge detector to segment blood vessels from the rest of the image.



Fig 9. A 2nd morphological filtering operation. An opening operation using a size-15 rectangular structuring element split objects that were connected by narrow strips and eliminated peninsulas from the edge detected image.



Fig 10. Post processing step 1: Color-to-gray-scale conversion. This is the result of the intermediate step of converting the color image to a binary

2nd Morphological filtering step (Algorithm 1): Next, Algorithm 1 smoothed the vessels through an opening operation using a large (size-15) rectangular structuring element. Using a large-sized structuring element helped extract the finer vessels in the image (see Fig. 9). This second morphological filtering step was done to split objects that are connected by narrow strips, and thereby eliminate extraneous peninsulas [4].

Post Processing (Algorithm 2): Algorithm 2, at this point, engaged an Arithmetic Mean filter to eliminate noise [4]. The Arithmetic Mean filter is a low pass filter that finds the average of the pixel values in its window and smoothes out local variations within the image [4] (see Fig 19).

Post Processing (Algorithms 1 & 2): Both algorithms converted the images from color, to gray scale, and then to binary images. Then, a logical NOT operation was performed (see Figs. 10-12 and 20-22).

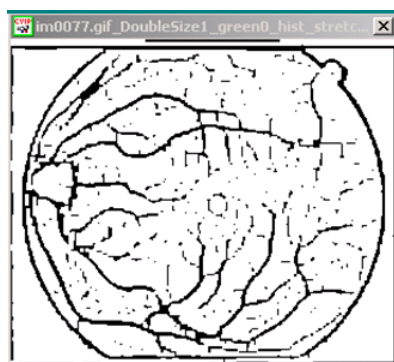


Fig 11. Post processing step 2: Gray scale-to-binary image conversion. The gray scale image has been converted to a binary image using a gray-level thresholding technique.



Fig 12. Post processing step 3: Logical NOT operation & Hough Transform. The NOT operation produced a black background. The Hough transform was used to attempt reintegration of bifurcation points and vascular branches



Fig 13. Ophthalmologist's hand-drawn image converted to a binary image for comparison to algorithms' output images.

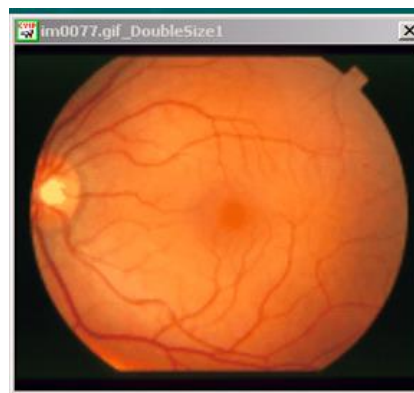
Algorithm 1: At this point, because Algorithm 1 had extracted most of the major and minor vessels with some missing intersections and bifurcations, a Hough transform was used to reintegrate vessel segments [4] (see

Fig 12). The Hough algorithm takes a collection of edge points (found by the Laplacian edge detector) and finds all the lines on which these edge points lie [4].

Algorithm 2: In Algorithm 2, an attempt was made to reconstruct missing vessel intersections by applying an edge-linking technique (See Figure 22). Edge linking connects edge points to create line segments and boundaries [4].



Fig. 14. Algorithm 2:
Original fundus image A
(150x130).



**Fig. 15: Algorithm 2: Resized original
image A (300x260)**



**Fig 16. Algorithm 2: Preprocessing
step 1.** Extraction of the green band
from the resized, original, color image
helped enhance image details.



**Fig 17. Algorithm 2: Preprocessing
step 2. The Y_p mean filter** eliminated
noise from the green band and
produced a smoothing effect.

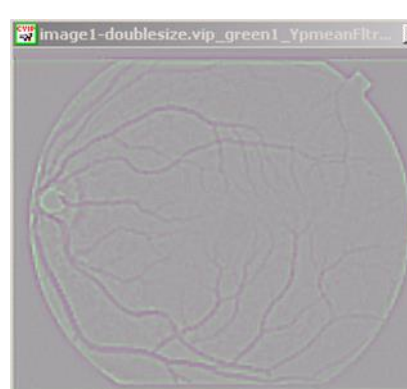


Fig 18: Algorithm 2: Edge detection.
Edges of the Y_p -mean filter-filtered
image were detected using a Laplacian
edge detector to segment blood vessels
out of the image.

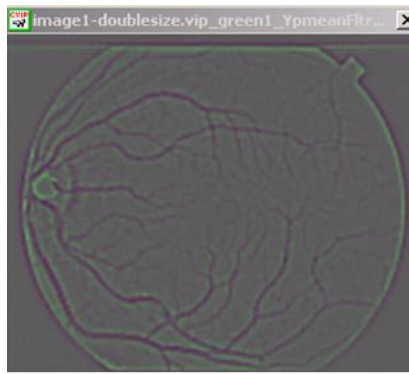


Fig 19. Algorithm 2: Post processing step 1. An Arithmetic Mean filter was applied to the edge-detected image to remove noise points.



Fig 20. Algorithm 2: Post processing step 2. Color-to-gray-scale conversion is the intermediate step to converting the color image to a binary image.



Fig 21. Algorithm 2: Post processing step 3. Grayscale-to-binary conversion: The gray scale image was converted to binary by using a binary threshold.



Fig 22. Logical NOT operation & edge linking. The NOT operation produced a black background with white objects. Edge linking was used to attempt reintegration of bifurcation points and vascular branches.



Fig 23: Binary-converted hand drawn image from the STARE database. It was first converted to gray scale, then binary thresholded at a gray-scale value of 75.

Conversion of the Ophthalmologist's Color, Hand-Drawn Images to Binary Images: The two algorithms' output images were analyzed for their extraction effectiveness by comparing them to the ophthalmologists' hand-drawn images. The algorithms' output images were in binary format. Consequently, the hand-drawn images were converted to binary format in order to make proper comparisons between them and the output images. The color hand-drawn images were first converted to gray scale images and then to binary images. The gray scale images were thresholded at a value of 75 (See Figures 13, 23, 25, 29 and 33).

Evaluation Tools: Pratt's Figure of Merit, Signal to Noise Ratio and Root Mean Square error are objective fidelity criteria that are used for measuring the amount of error in a reconstructed image by comparing it with a known image [4]. Objective fidelity criteria are not always correlated with our perception of an image's quality. For example, an image which has low error as determined by RMS error value may look worse than an image with high error value. These measures are useful for relative comparison of different versions of same image [4].

The algorithms were evaluated using the following quantitative measures to compare their output images with their corresponding hand-drawn images:

1. Pratt's Figure of Merit (FOM) measures the success of an edge detector by comparing the distances between edges in an original image to the edges in its edge-detected counterpart. It ranges from 0 – 1. The FOM for a missing edge is 0 (0% edges detected). For a perfectly-detected edges it is 1 (100%). The FOM takes into account the *types* of errors that can occur with edge detection methods. The types of errors are: 1) missing *valid* edge points, 2) *classifying noise pulses as valid* edge points, and 3) smearing of edges. If these errors do not occur, we can say that we have achieved success in edge detection.

The Pratt FOM, is defined as:

$$FOM = \frac{I_F}{I_N} \left(1 - \frac{\alpha}{N} \sum_{i=1}^N d_i \right)$$

where I_I is the number of ideal edge points in the image, I_F = the number of edge points found by the edge detector, I_N is the maximum of I_I and I_F , α is a scaling constant that can be adjusted to adjust the penalty for offset edges, and d_i is the distance between a found edge point to an ideal edge point

For this metric, the *FOM* will be 1 for a perfect edge. Normalizing to the maximum of the ideal (I_I) and found (I_F) edge points guarantees a penalty for smeared edges or missing edge points. In general, this metric assigns a better rating to smeared edges than to offset or missing edges. This is done because techniques exist to thin smeared edges, but it is difficult to determine when an edge is missed [4] [10].

2. Peak Signal-to-Noise Ratio (SNR) is used to measure the amount signal compared to the noise in the signal. Here, we use it to measure the amount of correct signal (correct segmentation) in the output image as it compares with the amount of segmentation inaccuracy (error). SNR is highest when the output image more perfectly matches the hand-drawn image. A higher SNR means there is more signal strength or more accurate segmentation in the output image [4].

$$SNR_{PEAK} = 10 \log_{10} \frac{(L-1)^2}{\frac{1}{N^2} \sum_{r=0}^{N-1} \sum_{c=0}^{N-1} [\hat{I}(r,c) - I(r,c)]^2}$$

where L is the number of gray levels in the image (e.g., $L = 256$ gray levels is facilitated by 8 bits)

3. The Root Mean Square (RMS) Error is found by taking the square root of the error squared divided by the total number of pixels in the image:

$$RMS = \sqrt{\frac{\sum_{i=1}^N (I_i - \hat{I}_i)^2}{N}}$$

RESULTS

Image A

Figure 26 shows the degree of match between Segmentation Algorithm 1’s output image A and its corresponding hand-drawn image. The degree of match using FOM, SNR and RMS error are 0.6506, 12.14 and 63.027, respectively. Figure 27 shows the degree of match between Segmentation Algorithm 2’s output image A and the corresponding hand-drawn image. The degree of match using FOM, SNR and RMS error are 0.6685, 10.536 and 65.81, respectively.



Fig 24. Original Image A (from the STARE database



Fig 25. Binary format of ophthalmologist’s hand-drawn tracing of blood vessels in Original Image A .

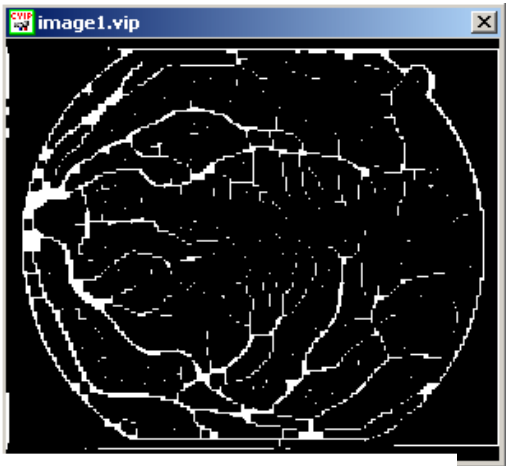


Fig 27. : Blood Vessel Segmentation Algorithm 2’s output image A. Degree of match to hand-drawn image using:
 Pratt’s figure of Merit: 0.6685
 Signal to Noise ratio: 10.536
 Root mean square error: 65.810

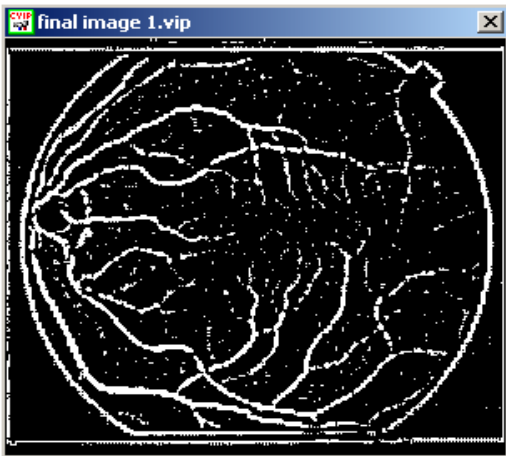


Image B

Figure 30 shows the degree of match between Segmentation Algorithm 1’s output image A and it’s corresponding hand-drawn image. The degree of match using FOM, SNR and RMS error are 0.5361, 11.11 and 70.967, respectively. Figure 31 shows the degree of match between Segmentation Algorithm 2’s output image A and the corresponding hand-drawn image. The degree of match using FOM, SNR and RMS error are 0.5577, 10.136 and 69.389, respectively.

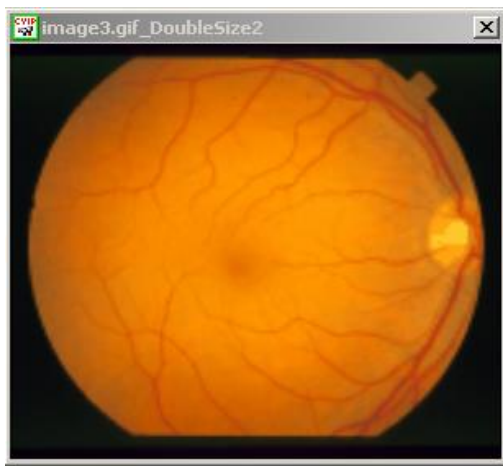


Fig 28. Original Image B.



Fig 29. Binary format of ophthalmologist's hand-drawn tracing of blood vessels in Original Image B.

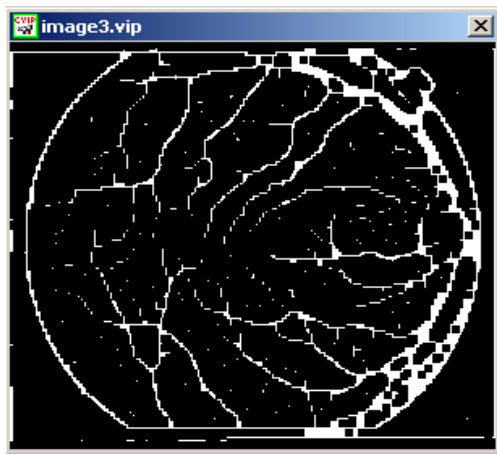


Fig 30. Blood Vessel Segmentation Algorithm 1's output image B. Degree of match to the hand-drawn image using:
Pratt's figure of Merit: 0.5361
Signal to Noise ratio: 11.11
Root mean square error: 70.967

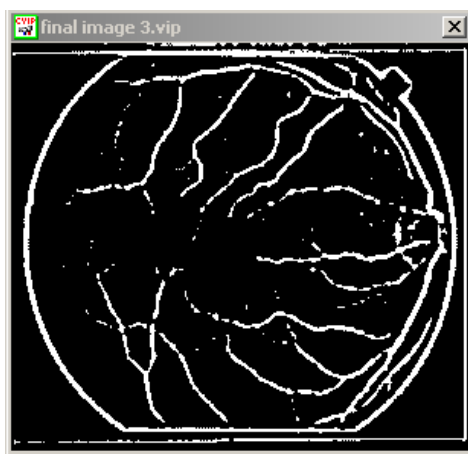


Fig 31. Blood Vessel Segmentation Algorithm 2's output image B. Degree of match to hand-drawn image using:
Pratt's figure of Merit: 0.5577
Signal to Noise ratio: 10.136
Root mean square error: 69.389

Image C

Figure 34 shows the degree of match between Segmentation Algorithm 1's output image A and its corresponding hand-drawn image. The degree of match using FOM, SNR and RMS error are 0.6481, 11.669 and 66.545, respectively. Figure 35 shows the degree of match between Segmentation Algorithm 2's output image A and the corresponding hand-drawn image. The degree of match using FOM, SNR and RMS error are 0.5822, 10.859 and 63.044, respectively.

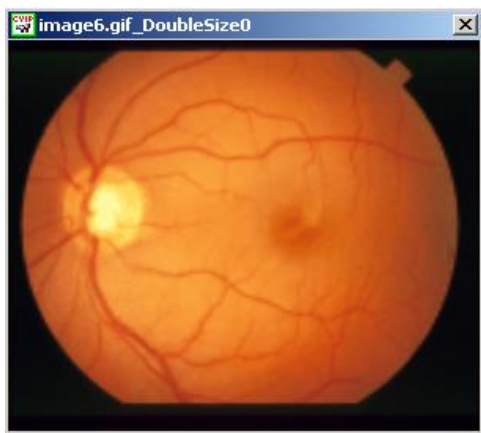


Fig 32. Original Image C.

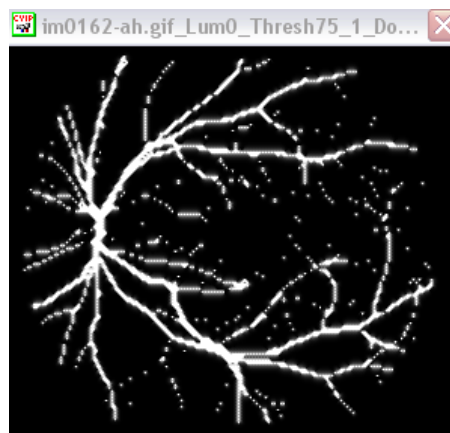


Fig 33. Binary format of ophthalmologist's hand-drawn tracing of blood vessels in Original Image C.

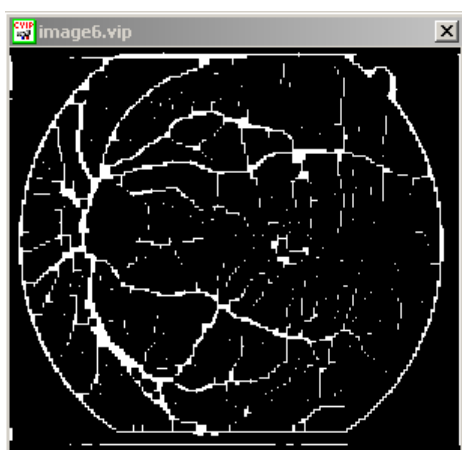


Fig 34. Blood Vessel Segmentation Algorithm 1's output image C. Degree of match to the hand-drawn image using:
Pratt's figure of Merit: 0.6418
Signal to Noise ratio: 11.669
Root mean square error: 66.545

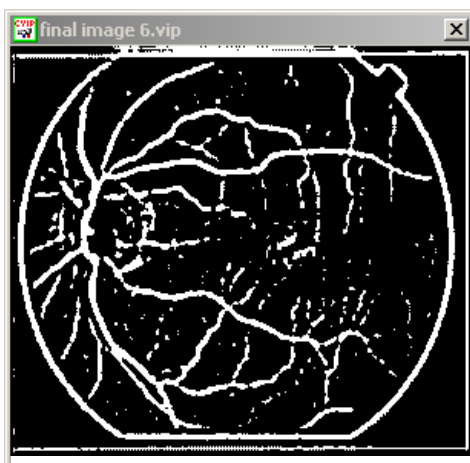


Fig 35. Blood Vessel Segmentation Algorithm 2's output image C. Degree of match to hand-drawn image using:
Pratt's figure of Merit: 0.5822
Signal to Noise ratio: 10.859
Root mean square error: 63.044

Table 1 and Figure 36 show the results of comparing the two algorithms' 15 output images to ophthalmologists' hand-drawn images using Pratt's Figure of Merit (FOM). The average FOM for the output images using Algorithms 1 and 2 are 48.84% and 54.27%, respectively. Table 2 and Figure 37 show the results of comparing the two algorithms' 15 output images to ophthalmologist's hand-drawn images using signal-to-noise ratio. The average SNR for the output images using Algorithms 1 and 2 are 11.404 and 9.959, respectively. Table 3 and Figure 38 show the results of comparing the two algorithms' 15 output images to ophthalmologist's hand-drawn images using the Root Mean Square Error (RMS). The average RMS Error for the output images using Algorithms 1 and 2 are 69.13 and 70.06, respectively.

DISCUSSION

The algorithms developed for automatic segmentation of blood vessels in fundus images using CVIPtools are experimented on 15 images from STARE database and the final results are compared with the hand drawn

images from the STARE database. Algorithm 1 segmented the image by filling out holes and smoothing out object outlines. However, some of the intersections are missing. We tried to reintegrate these missing intersections using the Hough transform. Even though the Hough transform applied, not all the missing vessels were integrated (see Fig. 12). Algorithm 2 extracted the blood vessels by histogram modification and edge detection followed by mean filtering to remove the noise. The obtained results are analyzed in terms of SNR (signal to noise ratio), RMS (root mean square) error and Pratt's figure of merit. For this metric FOM will be 1 for a perfect edge. This metric assigns a better rating to smeared edges than to offset or missing edges. In this method the ideal edge image, i.e., the hand drawn image is compared with edge detection image i.e., the final result and the scaling factor (1/9) is used to adjust the penalty of offset edges. Because some of the vessels are missing, error occurs when the final images are compared with binary converted hand drawn images. This error affects the signal strength. The outer ring is not eliminated, consequently contributing to the noise. This is one primary reason for high values of RMS error in both the algorithms. The final results obtained from the algorithms are binary images, whereas the hand-drawn images are color images. Consequently, the hand-drawn images were converted to binary format (color \rightarrow grayscale \rightarrow binary) at a gray-level threshold value of 75. During the course of the experiments, it was observed that better results could be achieved in terms of SNR, RMS error and FOM if the outer ring is eliminated.

Images	FOM for Algorithm 1	FOM for Algorithm 2
Image 1	0.6506	0.6685
Image 2	0.5361	0.5577
Image 3	0.6418	0.5825
Image 4	0.4877	0.5164
Image 5	0.5972	0.5429
Image 6	0.6197	0.5734
Image 7	0.4996	0.5800
Image 8	0.5102	0.5610
Image 9	0.3820	0.4453
Image 10	0.3421	0.4513
Image 11	0.4885	0.4961
Image 12	0.4414	0.5158
Image 13	0.3592	0.5245
Image 14	0.3503	0.5930
Image 15	0.4205	0.5328

Table 1. Results of comparing the two algorithms' 15 output images to ophthalmologists' hand-drawn images using Pratt's Figure of Merit (FOM). The average FOM for the output images using Algorithms 1 and 2 are 48.84% and 54.27%, respectively. On average, *Algorithm 2 has an FOM that is 10% higher than Algorithm 1.* (See the bar graph in Figure 37. below).

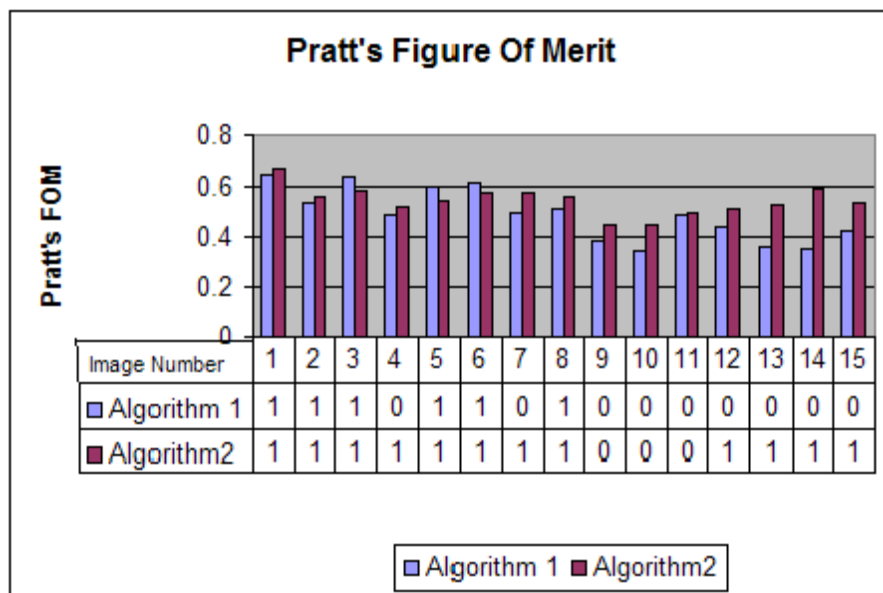


Fig 36. Bar graph comparing Pratt's Figure of Merit for retinal blood vessel segmentation using Algorithms 1 and 2 on 15 fundus images. The 15 sets of bars represent the performances of Algorithms 1 and 2 on 15 test images (horizontal axis). The table's bottom-most rows are the rounded FOM values for the two algorithms. FOM values > 0.5 has been approximated to 1 and FOM values < 0.5 have been approximated to 0.

Images	SNR for Algorithm 1	SNR for Algorithm 2
Image 1	12.14	10.536
Image 2	11.11	10.136
Image 3	11.669	10.859
Image 4	10.774	9.859
Image 5	12.952	9.055
Image 6	11.915	9.749
Image 7	12.296	10.419
Image 8	11.961	9.981
Image 9	10.595	9.736
Image 10	10.948	9.950
Image 11	10.166	9.016
Image 12	10.698	9.744
Image 13	11.747	10.124
Image 14	11.30	10.873
Image 15	10.794	9.356

Table 2. Results of comparing the two algorithms' 15 output images to ophthalmologists' hand-drawn images using signal-to-noise ratio (SNR). The average SNR for the output images using Algorithms 1 and 2 are 11.404 and 9.959, respectively. On average, *Algorithm 2 has a 6%-higher SNR than Algorithm 1.* (See the bar graph in Figure 38, below).

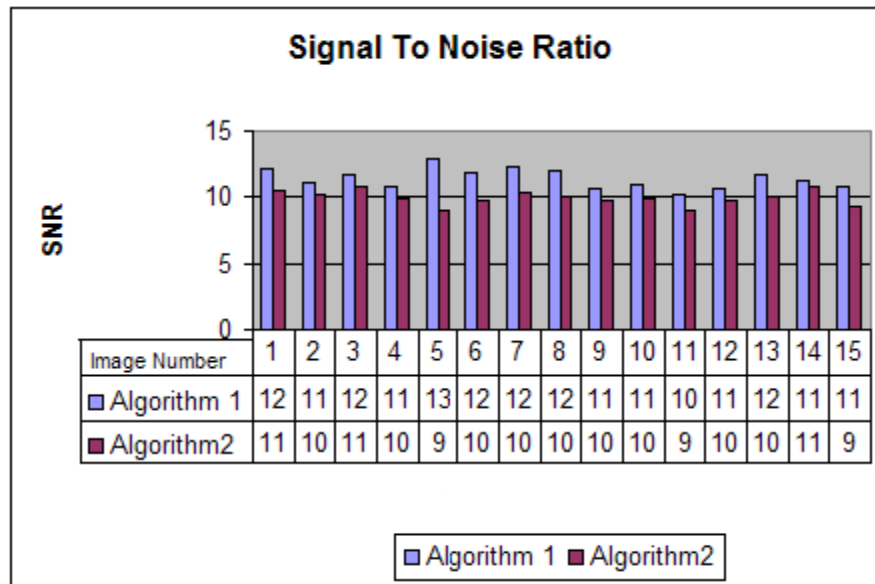


Fig 37. Bar graph comparing the signal-to-noise ratios for retinal blood vessel segmentation using Algorithms 1 and 2 on 15 fundus images. The 15 sets of bars represent the performances of Algorithms 1 and 2 on 15 test images (horizontal axis). The table's bottom-most rows are the rounded SNR values for the two algorithms. The images with SNR are approximated to their nearer values as shown in data table.

Images	RMS Error for Algorithm 1	RMS Error for Algorithm 2
Image 1	63.027	65.810
Image 2	70.967	69.389
Image 3	66.545	63.044
Image 4	73.760	71.773
Image 5	57.407	70.435
Image 6	64.684	73.000
Image 7	61.910	66.837
Image 8	64.339	70.814
Image 9	75.295	73.122
Image 10	72.303	71.105
Image 11	79.108	80.307
Image 12	79.730	73.048
Image 13	65.994	69.492
Image 14	69.429	62.924
Image 15	73.595	69.823

Table 3. Results of comparing the two algorithms' 15 output images to ophthalmologists' hand-drawn images using signal Root Mean Square error (RMS). The average RMS Error for the output images using Algorithms 1 and 2 are 69.13 and 70.06, respectively. On average, *Algorithm 1 has 1.3% more RMS error than Algorithm 2.* (See the bar graph in Figure 38, below).

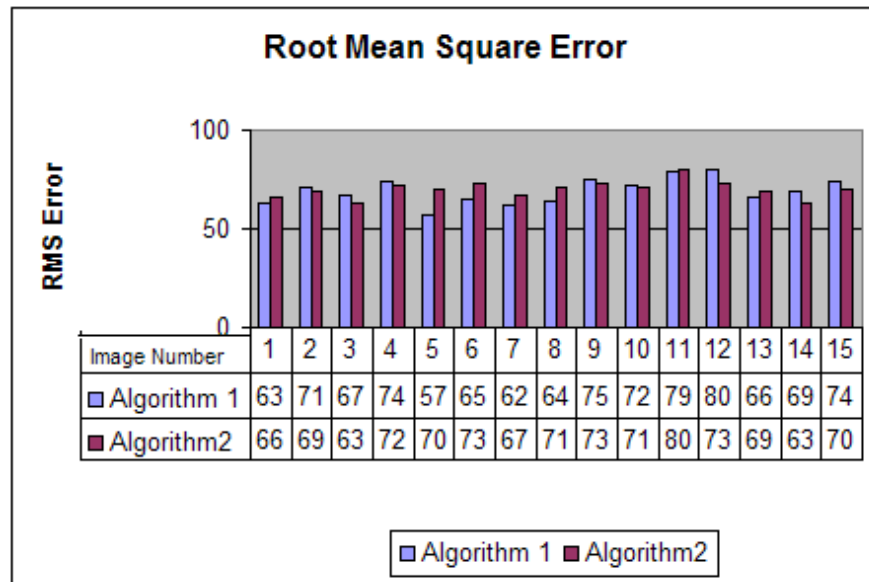


Fig 38. Bar graph comparing the Root Mean Square (RMS) Errors for retinal blood vessel segmentation using Algorithms 1 and 2 on 15 fundus images. The 15 sets of bars represent the performances of Algorithms 1 and 2 on 15 test images (horizontal axis). The table's bottom-most rows are the rounded RMS values for the two algorithms. The images with SNR are approximated to their nearer values as shown in data table.

SUMMARY

This paper proposed two algorithms for the automatic segmentation and detection of blood vessels in fundus images, using CVPitools. Both algorithms have been applied to fifteen images. The major difference between the algorithms' performances was that for both major and minor blood vessels, Algorithm 1 had difficulty segmenting intersections and bifurcations. Those junctions became lost in the output images. To recover them, we applied a reconstructive post-process using the Hough transform and edge linking. Although most of the major vessels' junctions could be recovered, most of the minor vessels' junctions could not. Algorithm 2 produced more consistent results, except that there is more "salt" noise in the output images.

CONCLUSION

Algorithm 1 extracted most of the major vessels, while Algorithm 2 extracted *all* of the major blood vessels and many of the minor ones.

From Figure 25-27, 29-31 and 33-35, it should be apparent by observation that both Algorithms 1 and 2 are extracting most (approximately 90-95%) of the vessels. Algorithm 2 has an FOM that is 10% higher than

Algorithm1. Algorithm 2 also has a 6%-higher SNR than Algorithm1. Although Algorithm 2 has 1.3% more RMS error than Algorithm 1, this comparative amount of error is negligible.

REFERENCES

1. Teng, T., Lefley, M., Claremont, D., Progress towards automatic diabetic ocular screening: a review of image analysis and intelligent systems for diabetic retinopathy, Medical and Biological Engineering and Computing, Vol. 40(1): 2-13, 2002.
2. Meadows, M., Saving your sight: Early detection is critical, FDA Consumer Magazine, March-April 2002. http://www.fda.gov/fdac/features/2002/202_eyes.html
3. Iqbal, M., Aibinu, A., Gubbal, N., *Automatic Diagnosis of Diabetic Retinopathy Using Fundus Images* (masters thesis), Bleking Institute of Technology, Karlskrona Sweden, 2006
4. Umbaugh, S.E., *Computer Imaging: Digital Image Analysis and Processing*, Boca Raton: CRC Press, 2005.
5. Fang, B., Hsu, W., Lee, M.L., Reconstruction of vascular structure in retinal images, IEEE International Conference on Image Processing, Vol. 2, Sept 2003.
6. Zana, F., Klein, J.C., Segmentation of vessel-like patterns using mathematical morphology and curvature evaluation, Proceedings of Computer Assisted Radiology and Surgery, Vol. 1281, May 2005
7. Al-Rawi, M., Qutaishat, M., Arrar, M., An improved matched filter for blood vessel detection of digital retinal images, Computers in Biology and Medicine, Vol. 37, Issue 2, February 2007.
8. Rapantzikos, K., Zervakis, M., Balas, K., Detection and segmentation of drusen deposits on human retina: Potential in the diagnosis of age-related macular degeneration, Medical Image Analysis, Vol. 7, March 2003
9. Abdel-Ghafar, R., Morris, T., Ritchings, T., Wood, I., Detection and characterisation of the optic disk in glaucoma and diabetic retinopathy, Proceedings of Medical Image Understanding and Analysis, September 2004
10. Pratt, W.K., *Digital Image Processing*, NY: Wiley, 1991.